Available online at www.sciencedirect.com
ScienceDirect
Journal of Power Sources 175 (2008) 749–759
JOURNAL OF POWER SOURCES
www.elsevier.com/locate/jpowsour

Influence of sorption kinetics for zirconia sensitization in solid oxide fuel cell functional anode prepared by electroless technique

Jayanta Mukhopadhyay, Madhumita Banerjee, Rajendra N. Basu *

Fuel Cell & Battery Division, Central Glass & Ceramic Research Institute, Kolkata 700032, India

Received 18 June 2007; accepted 21 September 2007
Available online 9 October 2007

Abstract

For preparation of solid oxide fuel cell functional anode (Ni-YSZ) by electroless deposition technique, surface adsorption of metallic palladium (Pd^0) on zirconia is the most important step during the sensitization process. For the sensitization process, the initial reaction kinetics are based on external mass transfer followed by intra-particle mass transfer phenomena. A kinetic model for the reversible sorption of Pd^0 on zirconia is developed that incorporates an effectiveness factor (η) which estimates the extent of intra-particle mass transfer. Based on the proposed model, an expression for Pd^0 uptake at equilibrium (p), an important property of YSZ, is developed. The theoretical kinetic model proposed is verified with experimental parameters like electrical properties of these functional anodes prepared under various sensitization conditions, e.g., agitation frequencies, equilibration time etc. Due to intra-particle mass transfer, the concentration gradient of Pd^0 from the surface of YSZ to bulk is minimized which favours uniform deposition of Ni on YSZ. Consequently, during subsequent electroless deposition of metallic Ni, the concentration gradient of the same is reduced from the bulk to the YSZ surface and results in enhanced functionality in the cermet anode. The validation is correlated with the electrical properties and surface morphologies of these functional cermets.

Keywords: Solid oxide fuel cell; Functional anode; Electroless deposition; Sorption kinetics

1. Introduction

For the anode-supported solid oxide fuel cell (SOFC), the most important cell component is the anode support. Apart from high electronic conductivity, anode should have sufficient interconnected porosity for proper percolation of the fuel and also to provide the effective number of electrocatalytic sites for oxidation of the fuel [1–3]. A functional anode with core–shell microstructures can reduce the Ni-content in the cermet even up to ~25 vol.% compared with 40 vol.% in conventionally prepared nickel–yittria stabilized zirconia (Ni–YSZ) cermet [4]. It is expected that these improved properties may help in reducing the mismatch of coefficient of thermal expansion between Ni and YSZ and may also solve the Ni coarsening problem during long-term SOFC operation [4–6]. The functional anode prepared by electroless technique involves an initial sensitization process which is the surface adsorption of metallic palladium (Pd^0) on YSZ under high energy ultrasonification. Power ultrasound has been found to have a profound influence on chemical reactions conducted in liquid phase, irrespective of whether they are homogeneous or heterogeneous in nature, and can cause a number of chemical effects [7–9]. This high-energy sonochemical reaction is used for sensitization of zirconia by surface adsorption of Pd^0 that forms instantaneously in the redox sensitization bath as follows:

$$SnCl_2 + PdCl_2 \rightarrow SnCl_4 + Pd^0 \quad (1)$$

Pd^0 adsorption on YSZ powder is an example of physisorption because metallic palladium is held by Van der Waals interaction with the YSZ precursor powder. Therefore, Pd^0 adsorption kinetics mainly involve two processes: (i) the external mass transfer of Pd^0 species from the bulk solution to the surface of YSZ and (ii) the intra-particle mass transfer of Pd^0 in the pores and on the YSZ surface [10]. An apparent kinetics

* Corresponding author. Tel.: +91 33 2473 3469/96x3507; fax: +91 33 2473 0957.
E-mail addresses: rnbasu@cgcri.res.in, rajenbasu@yahoo.ca (R.N. Basu).

0378-7753/$ – see front matter © 2007 Elsevier B.V. All rights reserved.
doi:10.1016/j.jpowsour.2007.09.109

takes into account the effects of both the chemical and physical rate processes and various physical process parameters, such as: (i) flow conditions, (ii) intensity of mixing and (iii) heat and mass transfer in the system, which can influence the kinetic rate [11–14].

The development of reversible sorption kinetics of the sensitization process is essential for understanding the basic mechanisms of surface adsorption of Pd^0 on YSZ particulates that govern the formation of core–shell structure in the functional cermet. The understanding of this physisorption process is mandatory for effective formation of the Ni shell around the YSZ core that enhances the functionality by increasing the overall triple-phase boundary length required for electrocatalytic oxidation of the fuel. This is reflected in the attainment of a transient equilibrium during the sensitization process. Various sensitization conditions, e.g., agitation frequencies, equilibration time etc will have a pronounced effect on the overall electrical properties of these functional anodes.

In the present investigation, a reversible kinetic model for the adsorption process during sensitization of YSZ is proposed and validated with relevant experimental evidence. In the present context, an effectiveness factor (η) has been introduced to estimate the effect of intra-particle mass transfer. This modification simplifies the evaluation of intra-particle mass transfer by avoiding consideration of the distribution of solute concentration in the pores of YSZ adsorbent.

2. Proposed kinetic model

2.1. Adsorption kinetics of Pd^0 on YSZ particulates

The adsorption process is mainly governed by the intra-particle mass transfer phenomena because the effect of external mass transfer can be eliminated by intensive agitation as will be shown in the subsequent sections. Intra-particle mass transfer involves not only surface and molecular diffusion but also diffusion in the pores of the particle. These effects can be expressed by an effectiveness factor (η) which can be defined as:

$$\eta = \frac{r_p}{r_s} \tag{2}$$

where r_s and r_p are the actual adsorption rate and the same evaluated at the outer surface condition, respectively [15].

2.2. Derivation of expression for r_s

YSZ sensitization process can be represented by the following equation:

$$\text{YSZ} + \text{Pd}^0 \rightarrow \text{YSZ–Pd}^0 \tag{3}$$

where YSZ–Pd^0 represents weak Van der Waals interaction between YSZ and Pd^0.

Applying the mass action law to the reaction given in Eq. (3), the rate of formation of YSZ–Pd^0 is given as

$$r_s = \frac{d[\text{YSZ–Pd}^0]}{dt} = k_1 e^{-E_1/RT}[\text{Pd}^0][\text{YSZ}] - k_2 e^{-E_2/RT}[\text{YSZ–Pd}^0] \tag{4}$$

Since the unoccupied surface active sites of YSZ are equal to the difference between the total active sites (YSZ_t) and the occupied surface active sites (YSZ–Pd^0), Eq. (4) can be written as

$$r_s = \frac{d[\text{YSZ–Pd}^0]}{dt} = k_1 e^{-E_1/RT}[\text{Pd}^0][\text{YSZ}_t - \text{YSZ–Pd}^0] - k_2 e^{-E_2/RT}[\text{YSZ–Pd}^0] \tag{5}$$

where [] denote the concentration (ppm) of the involved species, YSZ the adsorbent, Pd^0 the adsorbate, R the universal gas constant, T the experimental absolute temperature and k_1, k_2 and E_1, E_2 are the frequency (or pre-exponential) factors and activation energies for the forward and backward reactions, respectively, which are involved in the rate equation proposed by transition state theory.

Thus, Eq. (5) can also be written as

$$r_s = \frac{d[\text{YSZ–Pd}^0]}{dt} = k'_{ads}[\text{Pd}^0][\text{YSZ}_t - \text{YSZ–Pd}^0] - k'_{des}[\text{YSZ–Pd}^0] \tag{6}$$

where $k'_{ads} = k_1 e^{-E_1/RT}$ ($ppm^{-1}\,min^{-1}$) and $k'_{des} = k_2 e^{-E_2/RT}$ (min^{-1})

Eq. (6) could be further simplified as

$$p = [\text{YSZ–Pd}^0], \quad p_m = [\text{YSZ}_t], \quad q = [\text{Pd}^0]$$

$$r_s = k'_{ads} q(p_m - p) - k'_{des} p \tag{7}$$

Eq. (2) can now be written as

$$r_p = \eta r_s = \eta[k'_{ads} q(p_m - p) - k'_{des} p] \tag{8}$$

2.3. External mass transfer model

The external mass transfer model describes the change in adsorbate concentration with time. It can be expressed as

$$-\frac{dq}{dt} = k_f a_m (q - q_t) \tag{9}$$

where k_f is the mass transfer coefficient between the bulk solution and sorbent surface ($cm\,min^{-1}$), a_m the volumetric specific area of the adsorbent ($cm^2\,cm^{-3}$), q and q_t are the sorbate concentrations (ppm) in the bulk solution and at the surface of YSZ, respectively.

Assuming the YSZ particles to be spherical [16], an equation for volumetric specific area (a_m) can be written as

$$a_m = \frac{6m}{d_p \rho_p (1 - \varepsilon_p)} = \frac{6m}{d_p \rho_b} \tag{10}$$

where m, d_p, ρ_p, ρ_b, ε_p are the concentration ($g\,cm^{-3}$), the average size (μm), theoretical density ($g\,cm^{-3}$), bulk density ($g\,cm^{-3}$) and porosity of YSZ, respectively.

When external mass transfer is the controlling step, the surface concentration of metallic palladium (sorbate) is approximately constant. Taking the overall mass conservation into

consideration, the bulk concentration can be written as

$$q = q_0 - \frac{pM}{v} \tag{11}$$

where q_0, p, M and v are the initial concentration of Pd^{2+} (ppm) used (in the form of $PdCl_2$ solution), the Pd^0 uptake at equilibrium (ppm g^{-1}), the mass quantity of YSZ powder (g) and the water volume (ml) in the sensitized bath, respectively.

Substituting q, from Eq. (11) to Eq (9) gives:

$$\frac{dp}{dt} = \frac{vk_f a_m(q - q_t)}{M} \tag{12}$$

Using Eqs. (12) and (6), the expression for maximum adsorption capacity can be written as

$$r_s = \frac{d[YSZ{-}Pd^0]}{dt} = \frac{dp}{dt} = k'_{ads} q_t (p_m - p) - k'_{des} p = \frac{vk_f a_m(q - q_t)}{M}$$
$$\Rightarrow q_t = \frac{vk_f a_m q/M + k'_{des} p}{k'_{ads}(p_m - p) + k_f a_m v/M} \tag{13}$$

When the external mass transfer is the controlling step, i.e. $k_f a_m v/M \ll k'_{ads}(p_m - p)$ and $k_f a_m$ has a small value, Eq. (13) can be modified as

$$q_t = \frac{k'_{des} p}{k'_{ads}(p_m - p)} \tag{14}$$

Assuming the sorption isotherm to follow the Langmuir equation, expression for the Pd^0 uptake at equilibrium (p in ppm g^{-1}) can be written as

$$p = \frac{K_1 p_m q_s}{1 + K_1 q_s} \tag{15}$$

where K_1 is the equilibrium constant (ppm^{-1}), p_m the maximum sorption capacity of the sorbent (ppm g^{-1}) and q_s is the total Pd^0 concentration in solution (ppm).

Substituting Eq. (15) into Eq. (14) yields:

$$q_t = \frac{k'_{des} K_1 q_s}{k'_{ads}}$$

Given that $K_1 = k'_{ads}/k'_{des}$, the above equation can be written as

$$q_t = q_s \tag{16}$$

It is to be noted that Eq. (16) is applicable only at maximum adsorption capacity when it is considered that the total Pd^0 formed gets adsorbed on the sensitized YSZ surface.

As q_t is related to the equilibrium concentration, which is independent of time, Eq. (9) can be integrated with the following boundary conditions: at $t = 0$, $q = q_0$ (considering total reduction of Pd^{2+} to Pd^0); and at $t = t$, $q = q$:

$$\ln\frac{q_0 - q_t}{q - q_t} = k_f a_m t \tag{17}$$

2.4. Model solution of proposed adsorption kinetics

From Eqs. (8) and (11),

$$r_p = \eta r_s = \eta\left[k'_{ads}\left(q_0 - \frac{pM}{v}\right)(p_m - p) - k'_{des} p\right]$$
$$\Rightarrow \frac{dp}{dt} = \eta\left[k'_{ads}\left(q_0 - \frac{pM}{v}\right)(p_m - p) - k'_{des} p\right] \tag{18}$$

Integrating Eq. (18), the expression for Pd^0 uptake at equilibrium (p) can be written as

$$p = \frac{B/C - \sqrt{(B/C)^2 - (4A/C)} - \left\{(B/C) + \sqrt{(B/C)^2 - (4A/C)}\right\}\exp\left(2.303\ \eta\ t\ C\sqrt{(B/C)^2 - (4A/C)}\right)}{2\left[\exp\left(2.303\ \eta\ t\ C\sqrt{(B/C)^2 - (4A/C)}\right) - 1\right]} \tag{19}$$

where:

$$A = k'_{ads} p_m q_0 \tag{20}$$

$$B = -\left(\frac{k'_{ads} p_m M}{v} + k'_{ads} q_0 + k'_{des}\right) \tag{21}$$

$$C = \frac{k'_{ads} M}{v} \tag{22}$$

3. Experimental

The above proposed kinetic model is validated by the following experiments.

3.1. Particle-size distribution of YSZ adsorbent

Experiments were performed using two types of YSZ powder namely: (i) TZ-8Y, from Tosho Corporation, Japan (d_{50} ~0.2 μm and henceforth referred to as YSZ-Tosho), (ii) FYT from Unitech Corporation, UK (d_{50} ~3 μm and henceforth referred to as YSZ-Unitec). YSZ-Tosho was further processed to increase the d_{50} value to ~27 μm. In the present context, three different size fractions of YSZ powders were used to investigate the effect of particle size on the sorption kinetics of metallic palladium (Pd^0), which is the rate-controlling step for electroless deposition. Fig. 1 shows an inverse linear relationship between bulk density and particle size of the adsorbent (YSZ powders), from which it is clear that the bulk density decreases with increase in particle size of the YSZ powder.

3.2. Sorption kinetics with variable agitation frequencies

An adsorption study of Pd^0 on YSZ was carried out with the help of a high-energy ultrasonifier (BRANSON, SONIFIER 450) with an adjustable agitation frequency. While starting the process, the required amount of YSZ powder was added to a

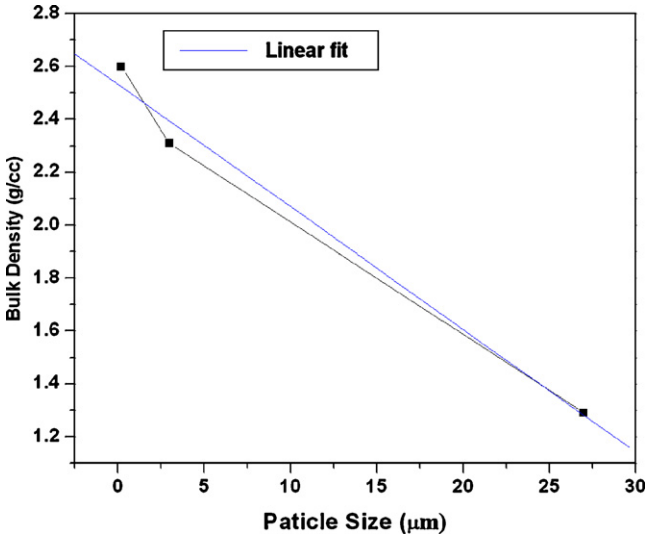

Fig. 1. Variation of bulk densities with particle size of YSZ powder.

redox bath that contained 0.001(M) palladium chloride solution and 0.265(M) stannous chloride solution. Metallic palladium (Pd^0), produced in situ (reaction given in Eq. (1)), was adsorbed on the YSZ surface upon placing the redox bath under a high energy ultrasonifier for 20 min at room temperature and in the agitation frequency range of 10–16 kHz. The sensitized bath was then kept for attaining equilibrium for effective adsorption of Pd^0 and complete precipitation of sensitized YSZ powder. In order to determine the adsorbed concentration of Pd^0 (q_t) on the YSZ surface, a certain aliquot from the supernatant solution of the sensitized bath was collected at a definite time interval and the residual concentration of Pd^{2+} in the supernatant solution was measured with the help of an inductive coupled plasma atomic emission spectrophotometer (Spectro Analysis Instrument, Kleve, Germany). The concentration of the adsorbed Pd^0 is calculated from the difference between the initial Pd^{2+} and the residual Pd^{2+} (in the supernatant liquid) concentration.

Adsorption being reversible in nature, simultaneous adsorption and desorption occur at the adsorbent surface and is generally known as sorption. The equilibration time is one of the crucial factors and is unique for a particular sorbent species. It is considered that the total Pd^0 formed during the sensitization process is adsorbed on the YSZ surface provided the sorbent is allowed to attain the transient equilibrium. However, the small amount of Pd^0 desorbed during the equilibrium sorption process is also taken into consideration during the reversible sorption kinetics.

3.3. Electroless deposition of Ni on to sensitized YSZ at different equilibration time intervals

The YSZ particulates sensitized at different time intervals of equilibration process were subjected to an electroless bath [4,5,17]. The flow chart of the process is shown in Fig. 2. The reaction bath is kept constant at ammoniacal pH and a temperature 80–90 °C. The reduction of Ni^{2+} from nickel nitrate solution was carried out by in situ liberation of the nascent hydrogen generated from a quantified addition of hydrazinehydrate.

3.4. Conductivity measurements of Ni–YSZ cermets

As-synthesized Ni–YSZ powders, prepared by electroless deposition on YSZ equilibrated in the sensitization baths for different periods of time, were mixed with 1.5 wt.% polyvinyl butyral (PVB) binder and pressed uniaxially in the form of green compacts of dimension 25 mm × 10 mm × 3 mm under a specific pressure of 170 MPa. The green compacts were sintered in air at a temperature of 1400 °C for 6 h. The sintered samples were then reduced at 1000 °C under a gaseous flow of argon and hydrogen (4:1) for 10 h and thus Ni–YSZ cermet bulk samples were produced. Conductivities of the reduced Ni–YSZ samples as a function of temperature were measured using standard 4-probe dc measurement technique using a 81/2 digit multimeter (Keithley, Model 2002). The corresponding conductivity values in various temperatures were then calculated using the formula:

$$\sigma = \frac{L}{Rbt} \tag{23}$$

where σ is the conductivity, R the 4-probe resistance of the samples measured, L the length between the two voltage probes, b the breadth and t is the sample thickness.

3.5. Surface morphologies of Ni–YSZ cermets at different equilibration time intervals

The highly polished microstructures of the Ni–YSZ functional cermets prepared with sensitized YSZ at different equilibration times of the adsorption regimes were observed with a high resolution optical microscope (Olympus GX 71, Japan). The microstructures of conventionally prepared Ni–YSZ cermets were also studied with the same microscope.

4. Results and discussion

4.1. Effect of particle size of YSZ on sorption kinetics

Kinetic experiments to study the effect of particle size of sorbent were carried out at the highest sonochemical agitation frequency of 16 kHz. It has been already mentioned that in the present context three different particle sizes of YSZ powder (0.2 μm, 27 μm of YSZ-Tosho and 3 μm of YSZ-Unitec) were used to study the size effect on the adsorption kinetics of Pd^0 on YSZ powder. The volumetric specific areas of the YSZ powders of varying particle size (0.2 μm and 27 μm of YSZ-Tosho and 3 μm of YSZ-Unitec) were determined from Eq. (10) and are summarized in Table 1. It is observed that with increase in particle size of adsorbent, the value of the bulk density decreases and thereby decreases the volumetric specific area, which is evident from Eq. (10).

Table 1
Determination of volumetric specific area of precursor YSZ powders (m = 0.0267 g cm^{-3})

Particle size (d_p) (μm)	0.2	3	27
Bulk density (ρ_b) (g cm^{-3})	2.6	2.3	1.3
Volumetric specific area (a_m) (cm^2 cm^{-3})	3081	231	46

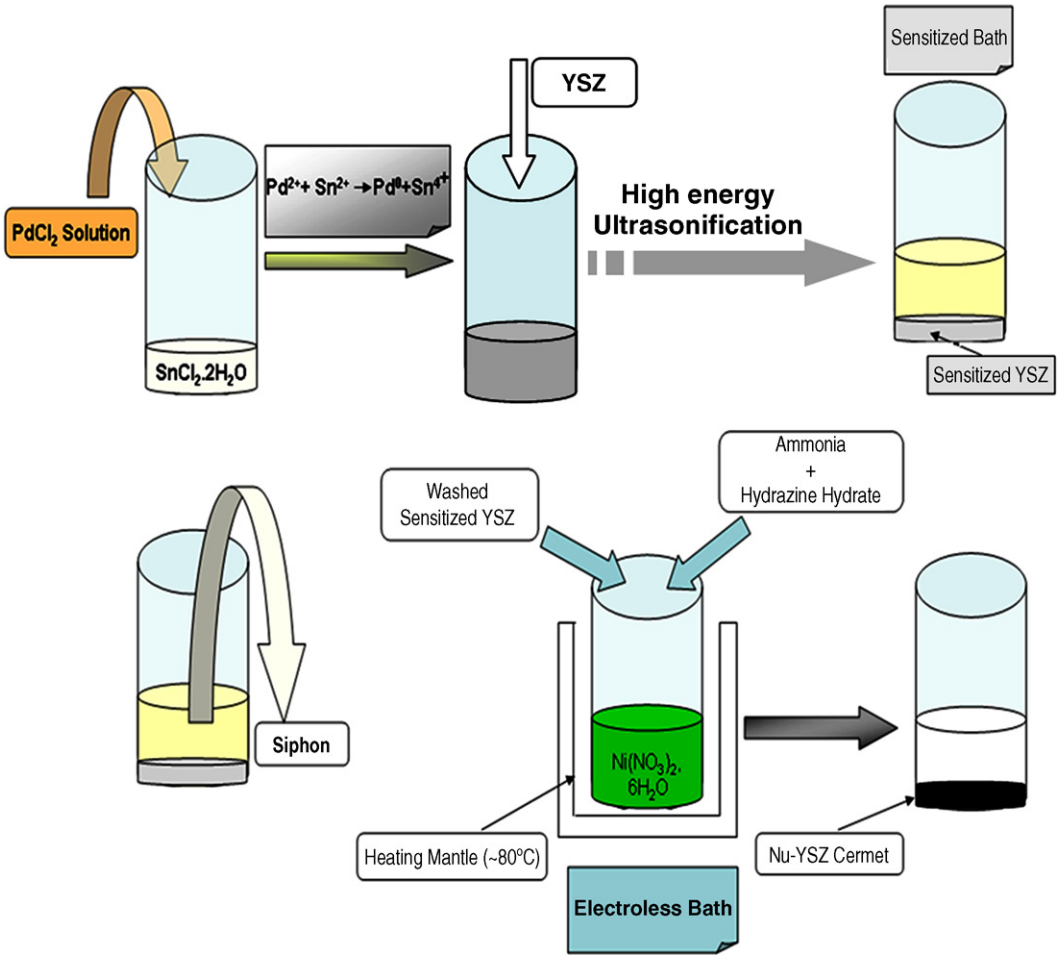

Fig. 2. Process flow chart for preparation of functional SOFC cermet.

Fig. 3 shows the dependence of the adsorption capacity (q_t) of YSZ with variation of time and establishes the particle size dependent equilibrium adsorption capacity (q_e). It can be concluded that specially treated YSZ-Tosho powder with particle size of 27 μm is most effective and optimum for surface adsorption of Pd^0, which is strongly supported from the highest equilibrium Pd^0 concentration value (q_e) of 95.243 ppm. With increase in particle size of the sorbent (from 0.2 to 27 μm), the uptake of Pd^0 increases. At this optimum size, the extent of physical Van der Waals interaction among the interacting species is expected to be strong enough and this results in better adsorption in comparison to smaller YSZ particle sizes.

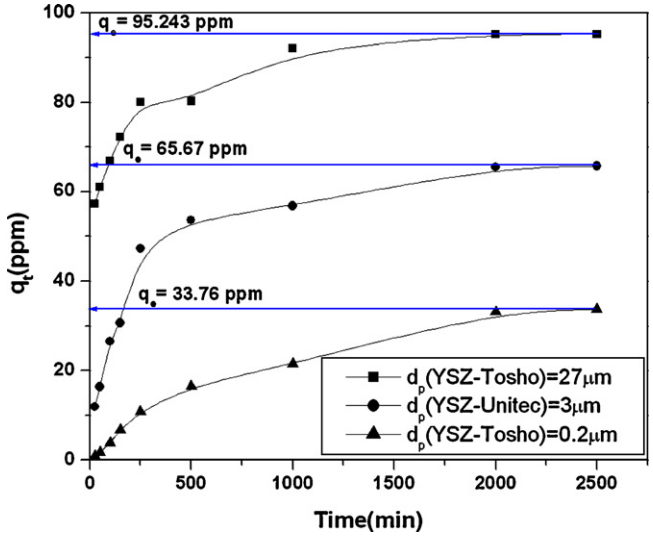

Fig. 3. Effect of particle size on adsorption kinetics (ν = 16 kHz).

4.2. *Effect of sonochemical agitation frequency on sorption kinetics*

Specially treated YSZ-Tosho powder ($d_p \sim 27$ μm) is most effective and optimum for surface adsorption of Pd^0, which is strongly supported from the highest equilibrium Pd^0 concentration value (q_e) as discussed in the previous section. Thus, the aforesaid experimental YSZ powder is used to study the effect of varying sonochemical agitation frequencies (10, 12, 14 and 16 kHz). The results in Fig. 4 shows that the sorption of Pd^0 by YSZ-Tosho powder is faster at higher frequency (16 kHz). It can be easily observed from the graph that in all cases, the equilibrium concentration value (q_e) of adsorbed Pd^0 approaches a constant value of 95.243 ppm but the equilibrium state is reached quickly at a relatively higher frequency. An increase in the adsorption rate with increase in agita-

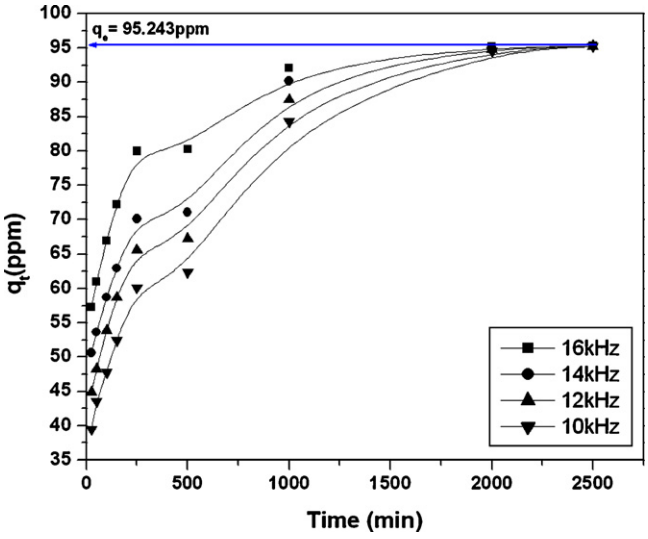

Fig. 4. Effect of agitation frequency on sorption capacity (q_t) of Pd^0 by YSZ-Tosho powder ($d_p \sim 27\,\mu m$).

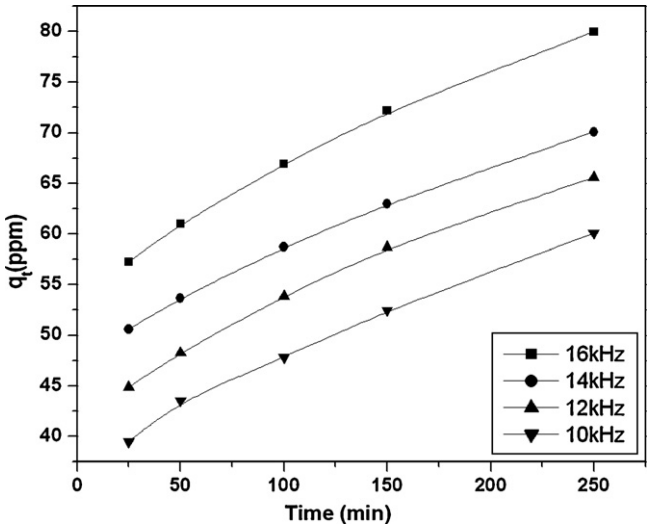

Fig. 5. Effect of agitation frequency on sorption capacity (q_t) of Pd^0 by YSZ-Tosho powder ($d_p \sim 27\,\mu m$) up to experimental time interval.

tion frequency can be explained by an enhanced turbulence in the solution (sensitized bath) which results in a decreased thickness of liquid boundary layer surrounding particles that leads to an increase in external mass transfer coefficient. At highest agitation frequency value of 16 kHz, the boundary layer becomes very thin and approaches a laminar sub-layer. Under these conditions, the external mass transfer resistance and coefficient values are almost constant and thus can be neglected.

4.3. Application of external mass transfer coefficient on sorption kinetics

Adsorption of Pd^0 on YSZ particulate is governed mainly by external mass transfer and intra-particle mass transfer phenomena. From Fig. 4, it is clear that depending on the time, the kinetics for Pd^0 adsorption proceeds at two different rates [18,19]. Initially (up to nearly 500 min), the adsorption proceeds very fast, which is indicated by a much steeper slope in the graph (Fig. 4). The high initial rate of Pd^0 uptake suggests that the adsorption occurs mainly at the sorbent (YSZ) surface and the external mass transfer plays an active role during this period of time. This is followed by a longer period of slower adsorption (plateau region in the graph) up to 2500 min. This behaviour indicates that the mechanism of intra-particle mass transfer (diffusion technique) is also involved in the sorption kinetic model and is represented by the slower adsorption rate, as mentioned above. The variation of external mass transfer governed sorption capacity (q_t) for the initial 250 min is shown in Fig. 5. It is clear that at the beginning of sorption, external mass transfer controls the process and the surface reaction is fast. With time, the driving force for external mass transfer in the pores decreases resulting from a decrease of Pd^0 concentration in the solution and, consequently, the mass transfer of metallic palladium becomes the main resistance. Fig. 5 is valid up to an equilibration time of 250 min where the change of adsorbate concentration with time according to the external mass transfer model follows first-order kinetics. An experimental linear fit of the external mass transfer model (Eq. (17)) for Pd^0 adsorption kinetics up to 250 min at different agitation frequencies is shown in Fig. 6. The values of the volumetric external mass transfer coefficient (k_v), which is equal to the product of the external mass transfer coefficient (k_f) and the specific area of the YSZ particle, are obtained from the slopes of Fig. 6 and are tabulated along with the corresponding k_f values in Table 2. It is observed that with increase in agitation frequency, the volumetric mass transfer coefficient increases and, therefore, for a particular YSZ adsorbent with a definite volumetric specific area, the external mass transfer coefficient increase which also supports that the adsorption regime is controlled primary by external mass transfer.

4.4. Application of intra-particle mass transfer model on sorption kinetics

To obtain the equilibrium constant (K_1) for Pd^0 adsorption on specially-treated YSZ-Tosho ($d_p \sim 27\,\mu m$) for the reaction given in Eq. (3), the Langmuir adsorption isotherm (Eq. (15)) is used and can be linearly expressed as

$$\frac{1}{p} = \frac{1}{p_m} + \frac{1}{K_1 p_m q_s} \tag{24}$$

$$\Rightarrow \frac{q_s}{p} = \frac{q_s}{p_m} + \frac{1}{K_1 p_m} \tag{25}$$

Eq. (25) is used to fit the data in Fig. 4; the results are given in Fig. 7. As the parameters in the Langmuir equation are governed

Table 2
The external and volumetric mass transfer coefficients at different agitation frequency ($d_p \sim 27\,\mu m$ and $a_m = 45.99\,cm^2\,cm^{-3}$)

Agitation frequency (kHz)	10	12	14	16
$k_{f\,exp}$ ($\times 10^{-5}$ cm min^{-1})	2.68	3.31	3.40	5.72
$k_{v\,exp}$ ($\times 10^{-3}$ min^{-1})	1.23	1.52	1.57	2.63

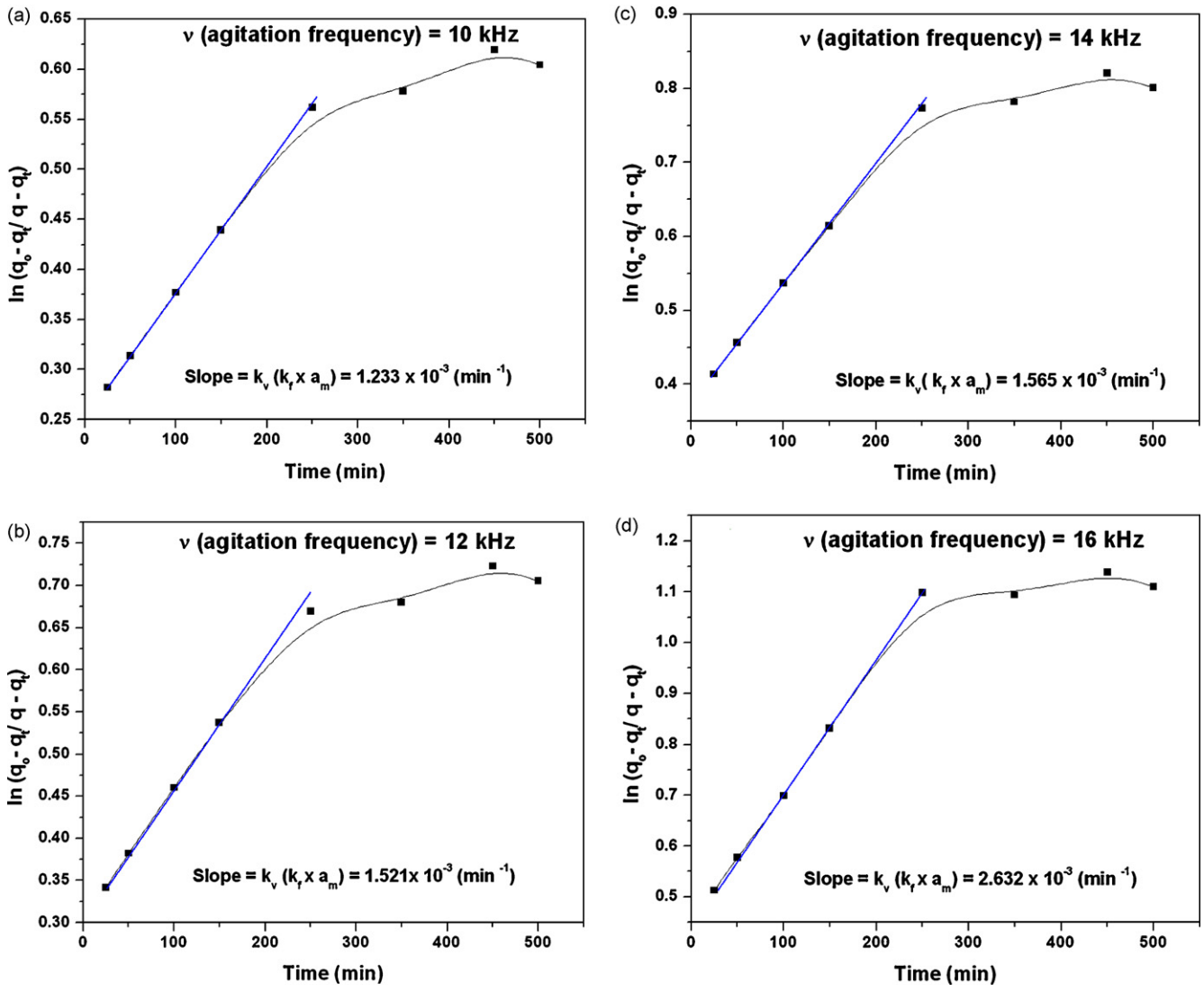

Fig. 6. Variation of $\ln(q_0 - q_t/q - q_t)$ vs. time for Pd^0 adsorption with agitation frequencies (ν) of: (a) 10 kHz, (b)12 kHz, (c)14 kHz and (d)16 kHz.

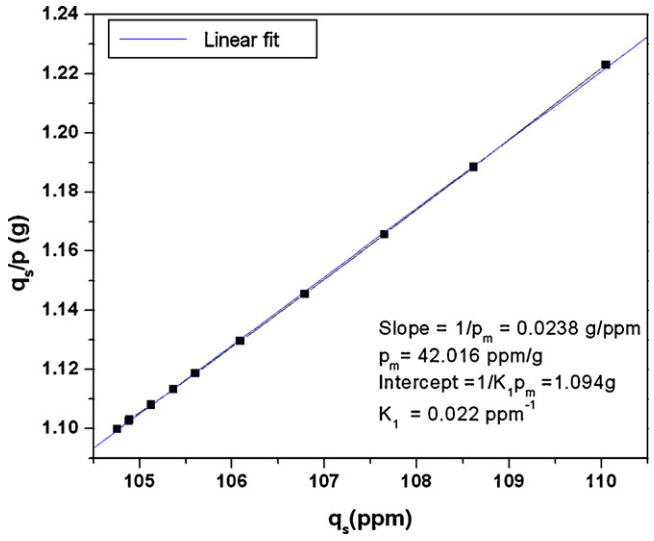

Fig. 7. Linear Variation of q/p vs. q.

by the equilibrium state of a time-dependent reversible process, Eq. (25) can only be applied in the transient equilibrium range (from 1000 to 2500 min) shown in Fig. 4. It can be seen from the linear fit of Fig. 7, that the Langmuir adsorption isotherm is valid in the latter stage of Pd^0 adsorption (Fig. 4), where the kinetics is governed entirely by intra-particle mass transfer phenomena and is responsible for the slower adsorption rate.

4.4.1. Determination of η (effectiveness factor)

For any reversible reaction as given in Eq. (3), the equilibrium constant can be written in terms of the forward and backward rate constants as

$$K_1 = \frac{k'_{\text{ads}}}{k'_{\text{des}}} \tag{26}$$

Therefore, using Eq. (26), Eqs. (20)–(22) can be modified as

$$\frac{B}{C} = -\left(p_{\text{m}} + \frac{q_0 v}{M} + \frac{v}{MK_1}\right) \tag{27}$$

Table 3
Comparative electrical conductivities of SOFC anodes prepared by different techniques

Temperature (°C)	Functional anodes		Conventional
	Transient equilibrated sensitized bath (28 vol.% Ni)	Non-transient equilibrated sensitized bath (37 vol.%Ni)	Solid state (40 vol.% Ni)
Conductivities of Ni–YSZ cermet (S cm^{-1})			
1000	264.54	205.82	149.11
800	489.59	486.19	505.73

and

$$\frac{A}{C} = \frac{p_m q_0 v}{M} \tag{28}$$

Considering the average equilibration time at 1750 min (Fig. 3) and $q = q_s$ in Eq. (15), theoretical adsorbate uptake at equilibrium (p) can be calculated from the Langmuir isotherm (Eq. (15)).

Using Eqs. (26)–(28) and the calculated value of p, Eq. (19) can be solved as

$$\eta k'_{ads} = 7.595\ \text{ml (g min)}^{-1} \tag{29}$$

$$\eta k'_{des} = 3.45 \times 10^{-4}\text{min}^{-1} \tag{30}$$

The physical significance of $\eta > 0$ is that diffusional resistances favour the forward reaction rate (adsorption) whereas, $\eta < 0$ promote the desorption rate [15]. Thus, from Eqs. (29) and (30), it can be proposed that the diffusion process (intra-particle mass transfer) not only favours the attainment of an adsorption equilibrium, but at the same time, it favours the adsorption rate. As $k'_{ads} >> k'_{des}$ (evident from Eqs. (29) and (30)) and η has a positive value in the equilibrium region of adsorption kinetics, the same is preferred over the backward desorption kinetics. Consequently, the concentration gradient of Pd^0 from the YSZ surface to the bulk is minimized and thereby reduces the Ni concentration gradient during subsequent electroless deposition from the bulk to YSZ surface, which, in turn, enhances the functionality of the materials for fuel cell applications.

4.5. Effect of equilibration time on enhancement of functionality

4.5.1. Electrical characterization

Fig. 8 shows the electrical conductivity values at 800 °C of SOFC functional anodes (prepared with transient and non-transient equilibrated sensitized bath) compared with those of the conventionally prepared anodes. The conductivity percolation threshold is brought down to ~28 vol.% Ni in the functional anode prepared with transient equilibrated sensitized bath in comparison with ~40 vol.% Ni for conventionally prepared samples. The functional anodes prepared with non-transient equilibrated sensitized bath does not show much improvement in lowering the vol.% of Ni in the cermet matrix for attaining the required upper percolation threshold for the electrical conductivity that is required for SOFC applications. The comparative electrical conductivities of functional and conventional anodes are given in Table 3.

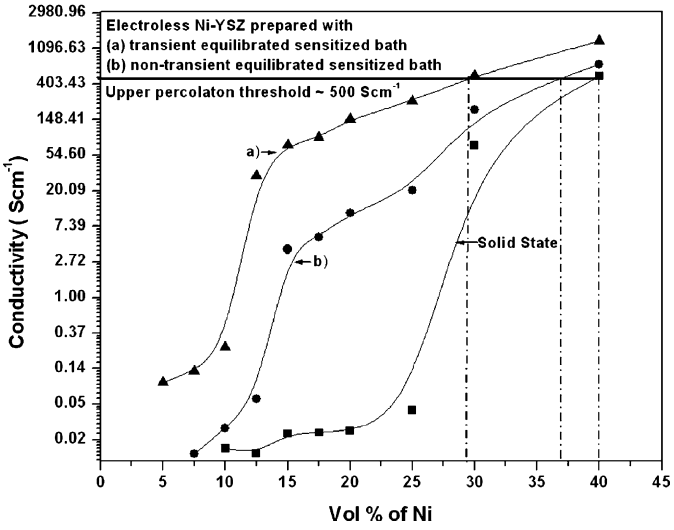

Fig. 8. Comparative electrical conductivities of Ni–YSZ cermet prepared by different techniques.

Arrhenius plots for the reduced Ni–YSZ samples for functional anodes prepared at transient and non-transient equilibrated state of sensitization are given in Fig. 9 and compared with that obtained from conventional solid-state synthesis. The corresponding activation energies for their conductivities are compared in Table 4. The nature of conduction is predominantly metallic. For the functional anode prepared with transient and non-transient equilibrated sensitized bath, conduction starts from 15 vol.% Ni onwards. For a conventional solid state synthesis, however, reasonable conductivity starts from 30 vol.% Ni. The important role of equilibration time during the sensitization process can be noted from the activation energies given in Table 4. The activation energy values for functional anodes prepared with transient equilibrated sensitized bath are less than those prepared from non-transient equilibrated sensitized bath

Table 4
Activation energies for electrical conductivities

vol.% of Ni content	15	20	25	28	30	37	40
E_{act} (kJ mol^{-1}), transient equilibrium	23.59	21.76	16.77	16.56	16.44	–	40.09
E_{act} (kJ mol^{-1}), non-transient equilibrium	38.01	36.24	33.17	–	32.96	32.71	36.09
E_{act} (kJ mol^{-1}), solid state	–	–	–	–	43.18	–	49.31

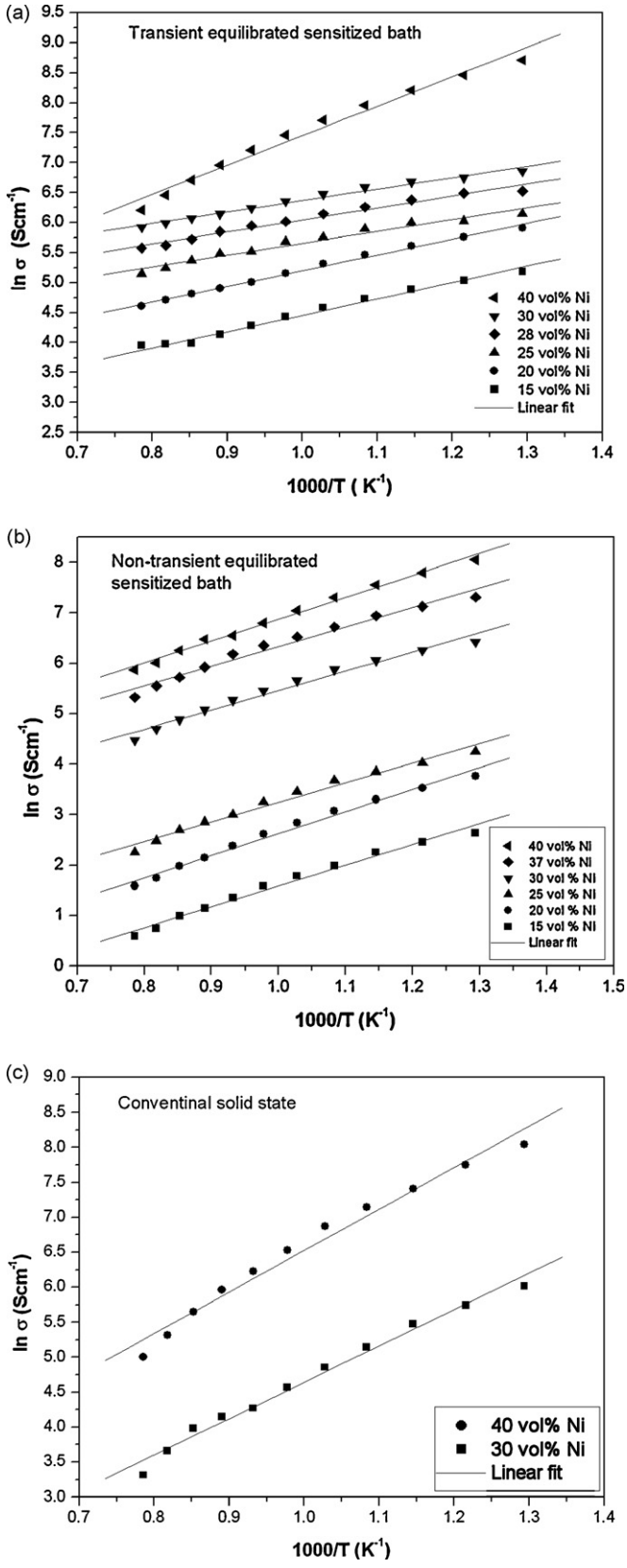

Fig. 9. Arrhenius plots of electrical conductivities as a function of nickel content for: (a) functional anodes prepared with transient equilibrated sensitized bath, (b) functional anode prepared with non-transient equilibrated sensitized bath and (c) conventionally prepared anode.

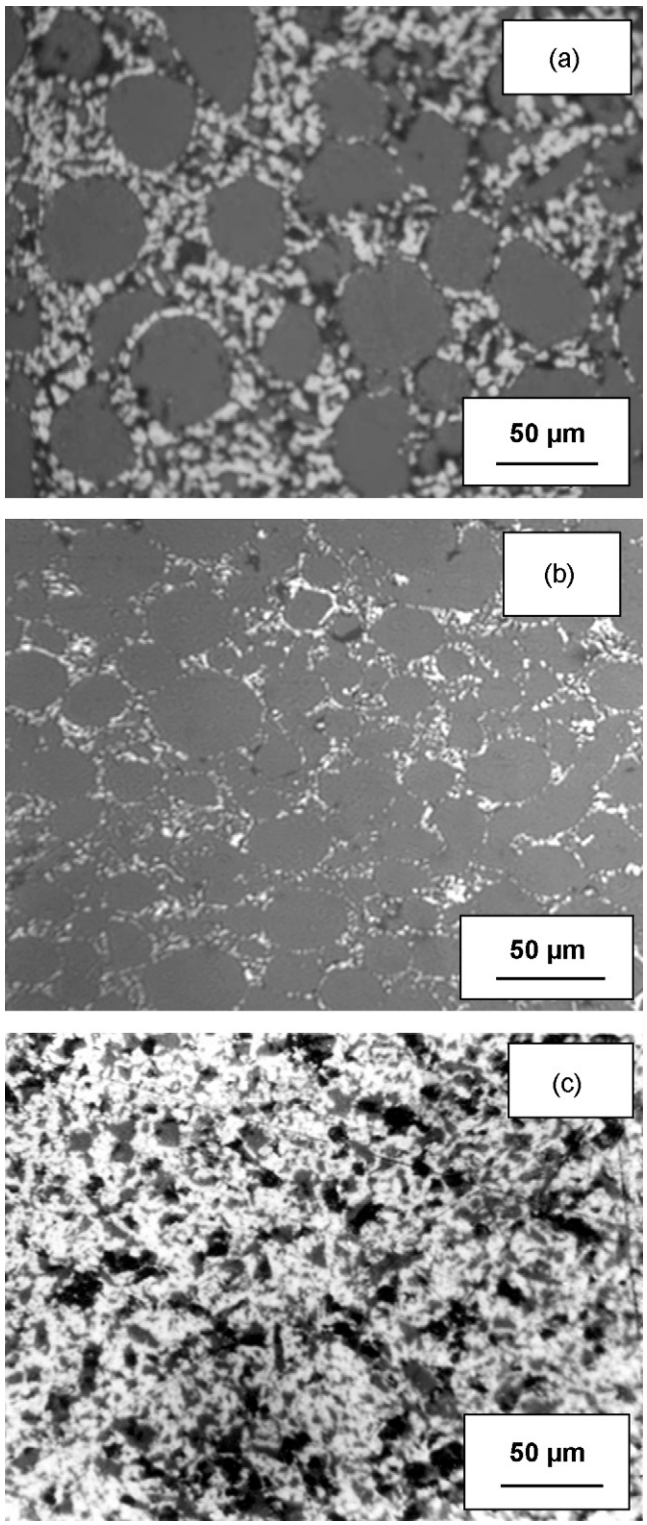

Fig. 10. Optical micrographs of functional Ni–YSZ cermet: (a) transient equilibrium adsorption, (b) non-equilibrium adsorption and (c) optical micrograph of conventionally prepared Ni–YSZ cermet.

up to 30 vol.% of Ni. From this observation, it may be concluded that in the former process, attainment of transient equilibrium leads to the formation of a prominent core–shell structure that makes the electronic path continuous in the cermets and thereby increases the conductivity at lower activation energy in comparison with the functional anodes prepared in a non-transient equilibrated state. By contrast, a reverse trend of activation energies in the functional anodes is observed at 40 vol.% Ni. Formation of a dense core–shell structure at 40 vol.% Ni in the functional anode prepared at a transient equilibrated state results in a higher rate of change of conductivity with temperature. This implies that the transient equilibrated sensitized bath favours the uniform formation of a Ni shell over the YSZ core, which is also supported by the proposed kinetic model.

4.5.2. Surface morphology

Fig. 10 compares the optical micrographs of the functional anodes prepared with transient and non-transient equilibrated sensitized bath with that of a conventionally prepared cermet. The core–shell microstructure is more prominent in Fig. 10a due to better sensitization of the YSZ particulate because of effective surface adsorption in comparison with Fig. 10b. This difference in the microstructure is due to the fact that in the first case, the sensitized bath is allowed to attain a transient equilibrium. This transient equilibrated sensitization process helps to encapsulate YSZ by freshly adsorbed Pd^0 which is evident from the positive value of the effectiveness factor of the proposed kinetic model. Thus, it is expected that because of the proper shell formation in this case, Ni distribution is more uniform across the thickness of the shell which, in turn, enhances the triple-phase boundary length required for fuel oxidation at the anode side. Compared to this functional anode, the microstructure observed in the case of the conventionally prepared cermet shown in Fig. 10c, is clearly visible as dispersed Ni in the YSZ matrix. Thus high energy sonochemical reaction contributes significantly to the effective surface adsorption of Pd^0 on zirconia that eventually enhances the functionality of Ni–YSZ cermet.

5. Conclusions

Ni–YSZ functional anode can be prepared by a novel electroless technique in which a sensitization process is the key step and involves surface adsorption of Pd^0 on to YSZ particulates. A sorption kinetic model with an effectiveness factor (η) is developed. It simplifies evaluation of the intra-particle mass transfer during the surface adsorption of Pd^0 on 8 mol% yttria stabilized zirconia (YSZ) powder under a high energy sonochemical reaction. Kinetic parameters such as effectiveness factor (η), time-dependent sorption capacity (q_t) and equilibrium sorption capacity (q_e) change with the particle size of the sorbent (YSZ). The reversible sorption kinetic model involves two processes: (i) external mass transfer and (ii) intra-particle mass transfer. The initial adsorption is preferably governed by external mass transfer but intra-particle mass transfer phenomena favour the attainment of an adsorption equilibrium. The external mass transfer coefficient depends on the agitation frequency but at a high value of 16 kHz, the effect of external mass transfer can be neglected after attaining equilibration. In this particular equilibrium adsorption regime, the sorption kinetics depend solely on intra-particle mass transfer since the sorption of Pd^0 on the YSZ surface is an example of physical adsorption.

Langmuir isotherm is used to fit the adsorption kinetics in the equilibrium adsorption region, where intra-particle mass transfer plays a major role. The equilibrium constant (K_1) and maximum adsorption capacity (p_m) values are determined from the Langmuir isotherm plot. The effectiveness factor (η) for Pd^0 adsorption is found to be positive which favours the forward adsorption rate in the equilibrium region where intra-particle mass transfer is the rate-controlling step. For preparation of a functional cermet anode of Ni–YSZ that is applicable for fuel cell anode materials, adsorbed Pd^0 on zirconia particulate acts as catalytically active sites for the reduction of Ni^{2+} to metallic Ni followed by subsequent formation of the uniform core–shell Ni–YSZ cermet. This is also reflected in the electrical conductivity values of functional anodes. Conductivities with transient equilibrated sensitized YSZ shows a prominence of Ni-shell formation across the YSZ-core and are correlated with optical micrographs. The experimental results validate the proposed sorption kinetic model with a positive effectiveness factor (η).

Supplementary data

Expression for adsorbate uptake at equilibrium.

Acknowledgements

The authors acknowledge the Director of CGCRI for his kind permission to present the work, Dr. Dipali Kundu of CGCRI, Kolkata for extending co-operation for ICP-AES measurements, and Dr. Abhijit Das Sharma, Scientist of Fuel Cell & Battery Division of the Institute for his valuable input. The authors also acknowledge CSIR-NMITLI project for financial support to conduct this research activity.

References

[1] S.C. Singhal, K. Kendall, High Temperature Solid Oxide Fuel Cells: Fundamentals, Design and Applications, Elsevier, 2003.
[2] R.N. Basu, S. Basu (Eds.), Materials for Solid Oxide Fuel Cells in Recent Trends in Fuel Cell Science and Technology, Anamaya Publishers, New Delhi, India, and Springer, New York, USA, 2006.
[3] N.Q. Minh, T. Takahashi, Science and Technology of Ceramic Fuel Cells, Elsevier, New York, USA, 1995, pp. 147–164.
[4] J. Mukhopadhyay, M. Banerjee, A. Das Sharma, R.N. Basu, H.S. Maiti, Electrochem. Soc. Trans. 7 (1) (2007) 1563–1572, The Electrochemical Society.
[5] S.K. Pratihar, A. Das Sharma, R.N. Basu, H.S. Maiti, J. Power Sources 129 (2004) 138–142.
[6] D.E. Dees, T.D. Claar, T.E. Easler, et al., J. Electrochem. Soc. 134 (1987) 2141.
[7] J.P. Lorimer, T. Mason, J. Chem. Soc. Rev. 16 (1987) 239–274.
[8] S.V. Ley, C.M.R. Low, Ultrasound in Synthesis, Springer, New York, 1989.
[9] K.S. Suslick, Scient. Am. 260 (2) (1989) 62–68.
[10] G.E. Boyd, A.W. Adamson Jr., L.S. Myers, J. Am. Chem. Soc. 69 (1947) 2836–2848.
[11] D.D. Do, Adsorption Analysis: Equilibria and Kinetics, Imperial College Press, 1998, 562 pp.

[12] D.M. Ruthven, Principles of Adsorption and Adsorption Process, 1984, pp. 199–200.
[13] J. Toth, Adsorption: Theory, Modeling and Analysis, Surfactant Science Series, vol. 107, 2002, 356 pp.
[14] W. Zhu, Advance Inductively Coupled Plasma—Mass Spectrometry Analysis of Rare Earth Elements, Environmental Applications, 1999, 65 pp.
[15] S.S.E.H. Elnashaie, S.S. Elshishini, Topics in Chemical Engineering, vol. 7, 1993, pp. 146, 153.
[16] Leusch, B. Volesky, J. Biotechnol. 43 (1995) 1–10.
[17] S.K. Pratihar, R.N. Basu, A. Das Sharma, H.S. Maiti, A process for preparing nickel yttria stabilized zirconia (Ni–YSZ cermet), Indian Patent (appl. no. 306/DEL/01 dated 27.02.2001).
[18] B. Wehrli, S. Ibric, W. Stumm, Colloids Surf. 511 (1990) 77–88.
[19] K. Kesenci, R. Say, A. Denizli, Eur. Polym. J. 38 (2002) 1443–1448.